Check for updates

Received: 2 July 2021 | Accepted: 20 July 2021

DOI: 10.1002/jccs.202100279

SPECIAL ISSUE PAPER

JCCS JOURNAL OF THE CHINESE CHEMICAL SOCIETY

Femtosecond relaxation dynamics of two-dimensional BiOI nanoplatelets as efficient photocatalysts

Atul H. Bhosale[1] | **Sudhakar Narra**[1,2] | **Sumit S. Bhosale**[1] | **Po-Sen Liao**[1] | **Nobuhiro Ohta**[1,2] | **Eric Wei-Guang Diau**[1,2]

[1]Department of Applied Chemistry, Institute of Molecular Science, National Yang Ming Chiao Tung University, Hsinchu, Taiwan

[2]Center for Emergent Functional Matter Science, National Yang Ming Chiao Tung University, Hsinchu, Taiwan

Correspondence
Nobuhiro Ohta and Eric Wei-Guang Diau, Department of Applied Chemistry and Institute of Molecular Science, National Yang Ming Chiao Tung University, 1001 Ta-Hseuh Rd., Hsinchu 30010, Taiwan.
Email: nohta@nctu.edu.tw and diau@mail.nctu.edu.tw

Funding information
Center for Emergent Functional Matter Science of National Yang Ming Chiao Tung University (NYCU); Taiwan Ministry of Science and Technology, Grant/Award Numbers: MOST 110-2634-F-009-026, MOST 109-2123-M-009-001

Abstract

The structural and optical properties of pristine and photoactivated surfaces of facet [001] of 2D BiOI nanoplatelet powders synthesized with an antisolvent method were studied using X-ray diffraction (XRD), a scanning electron microscope, X-ray photoelectron spectra (XPS), visible–near infrared (vis–NIR) absorption, and transient absorption spectroscopic techniques. The synthesized BiOI nanoplatelets possessed a tetragonal structure with length 200–400 nm and thickness less than 50 nm. XRD analysis showed that the photoactivation did not affect the crystal structure. In contrast, the XPS analysis showed vacancies associated with elements Bi, I, and O. The band gaps estimated from the diffuse reflectance spectra of pristine and photoactivated samples are 1.83 and 1.80 eV, respectively. Femtosecond transient-absorption spectra measured in the vis–NIR (2.25–0.9 eV) region showed photobleach bands associated with the band edge, shallow trap, and deep trap states. A global fit of the transient spectral profiles showed that all bands decay synchronously for both pristine and photoactivated samples, but the photoactivated samples showed a greater magnitude of carrier-carrier annihilation following photoexcitation due to photodoping caused by defects. A carrier-relaxation model involving thermal equilibrium between band-edge, shallow, and deep trap states is proposed to explain the synchronous decay of all bands.

KEYWORDS

BiOI, defects, oxygen vacancy, Tauc plot, transient absorption

1 | INTRODUCTION

Layered bismuth oxyhalides (BiOX) are among many novel promising two-dimensional materials that have applications in the fields of photocatalysis and photovoltaics.[1–7] BiOX belongs to semiconductors of the ternary (V–VI–VII) class with a tetragonal-matlockite structure in which a layer of $[Bi_2O_2]^{2+}$ is sandwiched between layers of halogen atoms with strong electrovalent bonds.[1–7] This unique arrangement leads to an asymmetric charge distribution between $[Bi_2O_2]^{2+}$ sheets and halogen sheets; as a result, an internal static electric field is produced perpendicular to the direction of the halogen atoms along the [001] facet of BiOX.[1–7] This internal electric field plays a prominent role in charge-carrier separation in BiOX photocatalysts, and is responsible also for their enhanced photocatalytic properties.[1–7]

Among BiOX, bismuth oxyiodide (BiOI), with its small band gap, serves as an ideal candidate for photovoltaic and photocatalytic applications as it can harvest more sunlight than other halides of this family. BiOI can

 © 2021 The Chemical Society Located in Taipei & Wiley-VCH GmbH

be grown in crystals of various shapes and sizes on varying the conditions of synthesis.[8–14] The optical and photocatalytic properties of BiOI also vary based on the synthetic conditions. The [001]-oriented BiOI exhibits an enhanced photocatalytic activity as charge separation is efficient along this direction.[8,11,15–17] Several low-temperature methods have been developed to grow BiOI along facet [001], as high-temperature methods typically lead to [010] orientations. When grown in the form of a thin sheet along [001], BiOI is highly advantageous, as thin sheets exhibit many surface defects, a decreased electron–hole diffusion length, and a large density of oxygen on the surface, which is generally suitable for the adsorption of reactants during photocatalytic reactions.[8,11,15–17]

Defects of both metal-based cationic type and oxygen-based anionic type play a prominent role in driving the photocatalytic reactions as conduction and valence bands are composed of metallic and nonmetallic orbitals, respectively.[5,7,18–21] When tuned appropriately, defects can thus modulate the electronic structure and enhance the range and intensity of absorption of the photocatalysts. Furthermore, photoirradiation effects before photochemical reactions can activate the surfaces on creating vacancies, so as to enhance the photocatalytic performance.[22,23] It is thus essential to understand the interplay of photoactivation processes in creating surface defects, which are crucial in charge separation and recombination that control the yields of photocatalytic reactions. Transient optical spectra have provided information on the dynamics of carrier relaxation, identifying traps, and their role in photocatalytic reactions of photocatalysts such as TiO_2,[24,25] but there are few such studies for BiOX-based photocatalysts. In earlier work, Wang et al. used transient visible absorption spectra to show that oxygen vacancies accelerate the charge recombination of excitons while oxygen-vacancy-mediated recombination occurs on nanosecond time scales for [001]-facet BiOBr nanoplates.[19] Similarly, Huq et al. used visible transient absorption spectra (TAS) to study the surface and bulk defect-mediated recombination in CVD-grown BiOI thin films.[26] Both these works described mechanisms of carrier relaxation based on the recovery of ground-state photobleach (PB) bands located in the visible region, but direct observations of shallow and deeptrap states, which are generally seen in the near-infrared (NIR) region, have yet to be observed; their role in carrier recombination is yet to be discussed.

In this work, we present the visible and NIR TAS results of [001]-facet pristine and photoactivated BiOI nanoplatelets synthesized via a novel antisolvent method. The synthesized two-dimensional nanoplatelet samples possessed a tetragonal structure; photoirradiation of these nanosheets activated their surfaces on creating vacancies. The TAS results showed also that photoactivated samples display dominant carrier-carrier annihilation processes due to photodoping caused by vacancies. A mechanism for carrier relaxation is provided at the end of this paper.

2 | RESULTS AND DISCUSSION

The structural characterizations of BiOI nanoplatelet powders synthesized with an antisolvent method are shown in Figures 1 and 2. Of samples of two types, one is pristine BiOI (yellow traces); the other is photoactivated BiOI (orange traces). The synthetic procedure is described in detail in the Section 4. The XRD patterns shown in Figure 1a confirm the formation of BiOI; the diffraction signals match satisfactorily the reported tetragonal structure.[8,9,17] The diffraction signals of (00k) orientations (k = 1, 2, 4, and 5) show intensities greater than those of (0k0) or (k00) orientations. This condition confirms that the synthesized nanoplatelets show a preferential growth along facet (001). As shown in Figure 1b, a BiOI nanoplatelet exposes oxygen sites along the desired (001) facet for enhanced photocatalytic activities. The SEM image of the synthesized BiOI powders (Figure 1c) shows a two-dimensional nanoplatelet structure of length 200–400 nm and thickness <50 nm, similar to the results published elsewhere.[17,27,28]

The Kubelka-Munk functions ($F(R_\infty)$) of BiOI samples obtained from their corresponding reflectance spectra are shown in Figure 1d with the absorption increasing above 2 eV. According to the Kubelka-Munk theory, the absorption spectra of powder samples are obtained from their diffuse reflectance spectra on calculating Kubelka-Munk function $F(R_\infty)$, which is given by

$$F(R_\infty) = \frac{K}{S} = \frac{(1-R_\infty)^2}{2R_\infty} \quad (1)$$

here, K and S are absorption and scattering coefficients; $R_\infty = \frac{R_{\text{sample}}}{R_{\text{standard}}}$ is reflectance of a sample of infinite thickness. The direct and indirect band gaps were deduced on substituting $F(R_\infty)$ into the Tauc equation (2).

$$(F(R_\infty).h\nu)^{1/\gamma} = B\left(h\nu - E_g\right) \quad (2)$$

here, B is a parameter, E_g is the band gap, and γ is a factor equal to ½ or 2 for direct or indirect transitions, respectively.[29,30] The direct and indirect band gaps obtained from Equation (2) for the BiOI sample are 2.19 and 1.83 eV, respectively. The band-gap values of BiOI samples are typically sensitive to the synthetic procedure

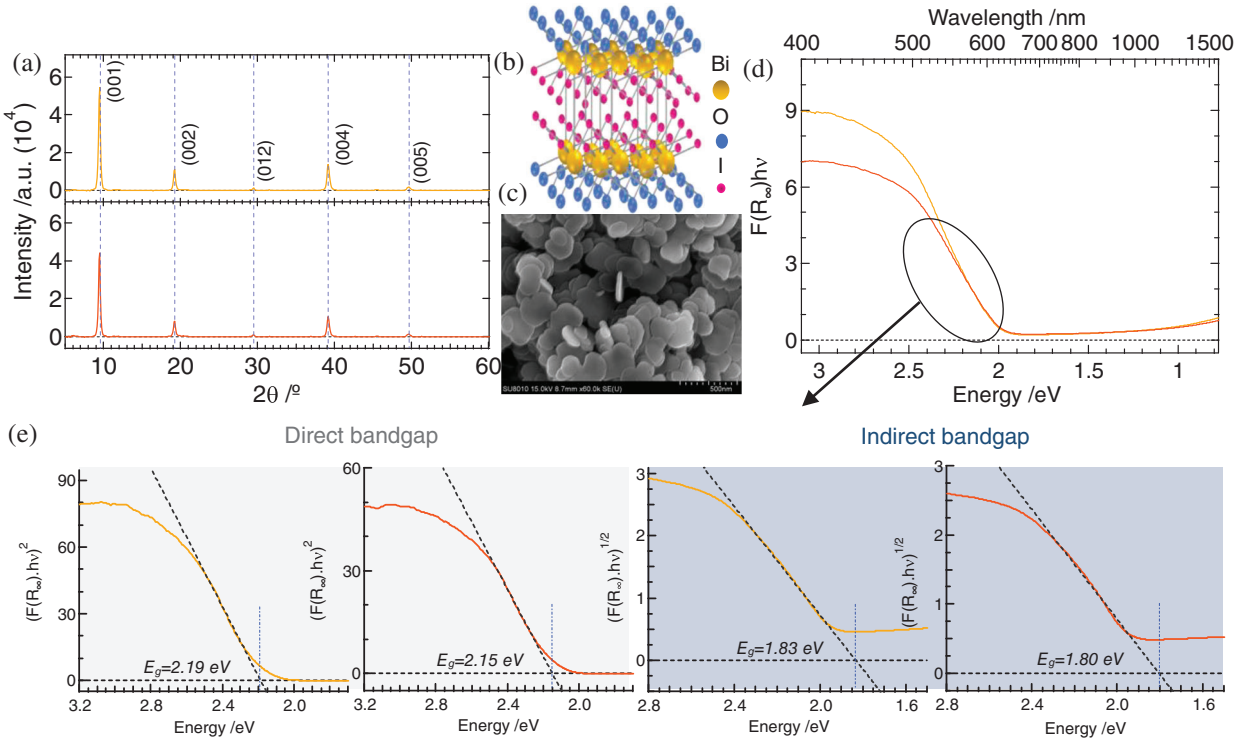

FIGURE 1 (a) X-ray diffraction (XRD) patterns of (——) pristine and (——) photoactivated BiOI samples. (b) Schematic of BiOI showing growth along direction (001). (c) Scanning electron microscope (SEM) image of BiOI nanoplatelets. (d) Diffuse reflectance spectra of (——) pristine and (——) photoactivated BiOI samples. (e) Tauc plots determining direct and indirect bandgaps for pristine (——) and photoactivated (——) BiOI samples

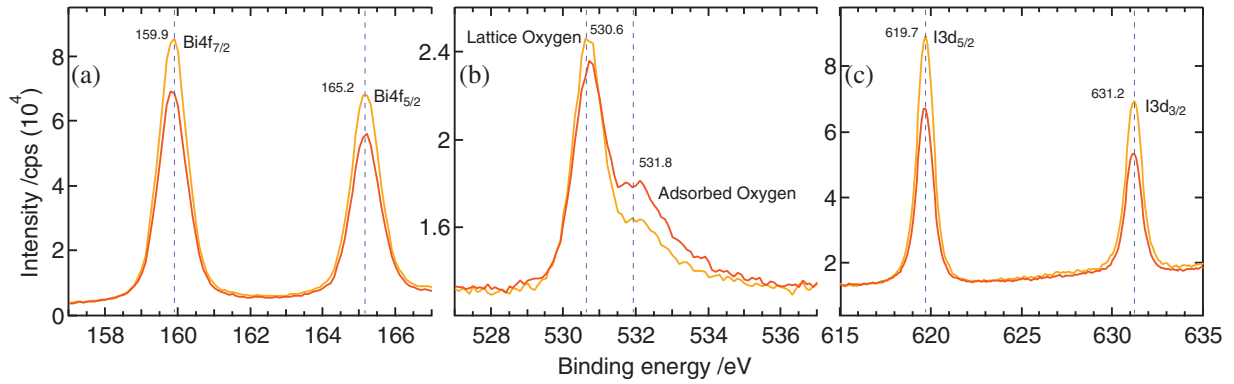

FIGURE 2 High-resolution X-ray photoelectron spectra of Bi (a), O 1*s* (b), and I 3*d* (c) elements for (——) pristine and (——) photoactivated BiOI NP samples

and the thickness of the films.[31] The values of E_g determined for the BiOI NP sample in this report are consistent with the literature.[4,31]

High-resolution X-ray photoelectron spectra (XPS) of BiOI nanoplatelet samples shown in Figure 2 display signals associated with elements Bi 4*f* (Figure 2a), O 1*s* (Figure 2b), and I 3*d* (Figure 2c). The XPS of Bi show two lines associated with Bi^{3+} $4f_{7/2}$ and $4f_{5/2}$ at ~159.9 and 165.2 eV, respectively. The XPS of O 1*s* show a line associated with lattice oxygen (O^{2-}) at 530.6 eV with a shoulder at 531.8 eV; this shoulder is generally associated with surface-adsorbed oxygen or anti-site-substituted oxygen atom.[15] XPS of oxygen also show surface-adsorbed water molecules at energy above 532 eV. The BiOI nanoplatelets studied here were carefully dried and showed no strong signature associated with surface-adsorbed water molecules. The XPS of I also show two lines associated with I^- $3d_{5/2}$ and $3d_{7/2}$ at ~619.7 and 631.2 eV, respectively. Our BiOI XPS results agree satisfactorily with the literature.[15,17,26,28] This XPS analysis shows that the synthesized BiOI nanoplatelets formed with a low-temperature method have surface-active oxygen or anti-site-substituted oxygen atoms,

which might promote the efficiency of photocatalytic experiments.

The photocatalytic effects on the structure and kinetics of the BiOI samples were investigated on irradiating the samples with a Xe lamp (150 W) for 12 hr. The XRD patterns of the photoactivated samples shown in Figure 1a indicate no change of the crystal structure except decreased diffraction intensities. The Kubelka-Munk function and XPS lines also showed a decreased intensity for a photoactivated BiOI sample, as can be seen from Figures 1d and 2. The direct and indirect bandgaps estimated from Tauc plots shown in Figure 1e of the photoirradiated sample are 2.15 and 1.80 eV, respectively. The direct and indirect band gaps of the photoactivated sample are smaller than those of a pristine sample (Figure 1e). These cumulative observations from XRD, absorption, and XPS indicate that the decreased intensity might be due to the formation of vacancies. The observations from XPS of photoactivated samples shown in Figure 2 indicate that iodine atoms are displaced more than bismuth and oxygen. The increased signal of surface-adsorbed oxygen for the photoactivated sample indicates that oxygen is more likely to adopt an anti-site substitution with iodine, as an oxygen atom is smaller than an iodine atom. This condition indicates also that the signal of surface-adsorbed oxygen observed in the pristine sample might also be due to anti-site-substituted oxygen atoms, similar to the photoactivated sample. According to theoretical calculations, bismuth and iodine vacancies lead to shallow defects whereas oxygen vacancies and bismuth anti-site substitution with iodine lead to deep traps.[5,26,32] The XPS of Bi 4*f* shown in Figure 2a do not support anti-site substitution, unlike O 1*s* shown in Figure 2b. The most likely defect states formed in our BiOI samples are shallow defects caused by vacancies of Bi, I, and O_I, along with a deep defect caused by the vacancy of an O atom.

The effects of the shallow and deep trap defects on the dynamics of carrier recombination of the BiOI samples were further investigated using femtosecond TAS. The TA spectra of pristine and photoactivated BiOI samples are shown in Figure 3. The TA experiments were performed on exciting the samples at 490 nm and probing in the visible and near-IR regions spanning 550–1,300 nm (2.25–0.9 eV). The TA spectra of pristine and photo-activated samples show broad PB bands spanning all probed regions. The evolution of PB bands occurred within a few hundred femtoseconds; subsequent recombination occurred in the sub-nanosecond regime. The TA spectra that we recorded for facet (001) of the BiOI samples are similar to those of the CVD-grown, randomly oriented BiOI samples reported elsewhere.[26] The broad PB bands observed for BiOI samples were attributed to flattened dispersion of the valence band along with closely lying direct, indirect, and shallow-trap states.[26] To distinguish between these various transitions is difficult. The overlap of several transitions can be realized through the observation of a weak positive photoinduced absorption (PIA) band after the recovery of the PB bands for both pristine and photoactivated samples. The long-lived and weak PIA band must hence be a signature of shallow traps. Theoretical calculations indicate that vacancies due to Bi and I and anti-site substitutions of O_I lead to shallow trap states that are resonant at or near band edges.[5,26,32] The recombination periods from shallow traps are typically greater than band-to-band recombination as trapping and detrapping processes retard the recombination mediated by shallow trap states. This assignment of the long-lived PIA band to a shallow trap state is thus reasonable.

The PB bands observed in the near-IR part of the TA spectra indicate depletion from deep trap states according to transient spectral results published elsewhere.[33] The PB bands observed for deep traps indicate that defects of electron-donating type form these traps, possibly anions (O^{2-}), as the population is depleted following photoexcitation. The TAS results for the existence of shallow and deep defects thus agree satisfactorily with the XPS results reported above. The photo-activated effect on the TA spectra of BiOI samples was not prominent. The slight difference observed in the spectral shape in the visible region of both samples might be due to a rearrangement of the density of shallow defect states followed by photoirradiation.

As shown in Figure 4a–c, the transient profiles of band-edge carriers, shallow, and deep trapped carriers were monitored at 1.77, 1.46, and 1.08 eV, respectively, for both pristine and photoactivated samples. The observed kinetics were fitted to a triple exponential function; the fitted results are summarized in Table 1. All transient decay profiles were fitted to the same set of time coefficients, 15 ps (τ_1), 152 ps (τ_2), and 6 ns (τ_3), with changes only in the pre-exponential factors depending on the probed wavelength. A global-fit analysis was performed on the transient kinetics with each 10-nm interval according to the results summarized in Table 1; the pre-exponential factors are indicated in parentheses. The results of the global fit are shown in Figure S1. The TAS of pristine and photoactivated BiOI samples are decomposable into three features based on the pre-exponential factors of the fitted function, namely hot carriers, cold carriers in shallow trap states, and cold carriers in deep trap states. A comparison of TA spectra between pristine and photoactivated samples is shown in Figure S1a, for which photoirradiation slightly altered the band curvature and increased the photodoped carriers. The change of band curvature between the two samples is discernible from the smaller blue shift and smaller amplitude

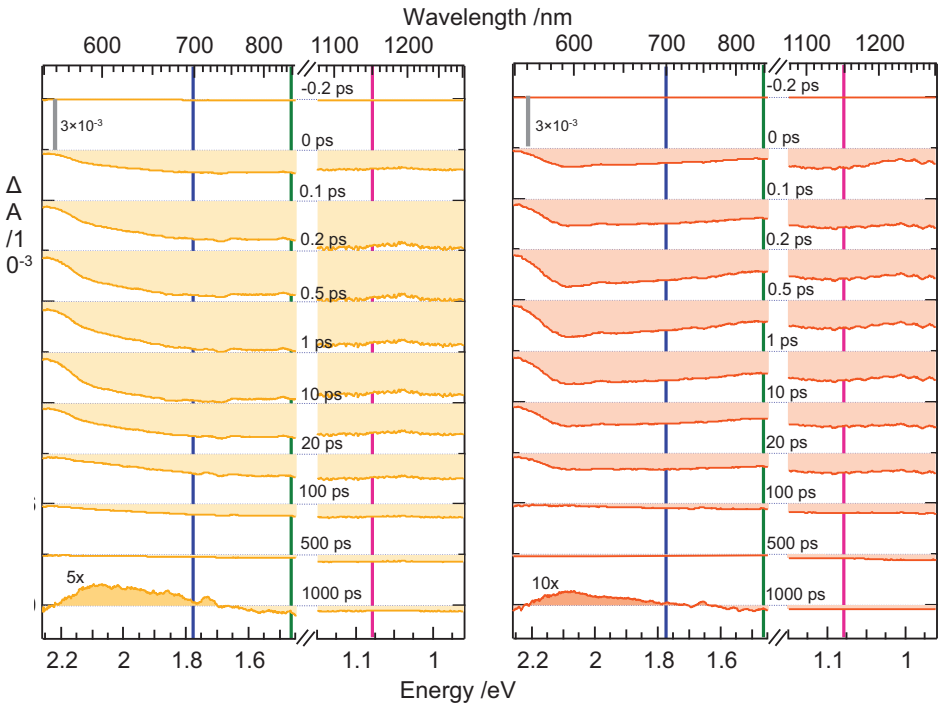

FIGURE 3 Femtosecond transient absorption spectra of pristine (——) and photoactivated (——) BiOI samples obtained on photoexciting the samples at 490 nm. The laser fluence was set to 200 μJ/cm^2. The time-resolved spectra are offset by factor 3×10^{-3} for clarity. The TA spectra observed at 1,000 ps are amplified by factors 5 and 10, respectively, for pristine and photo-irradiated samples so that weaker PIA bands from shallow traps are discernible

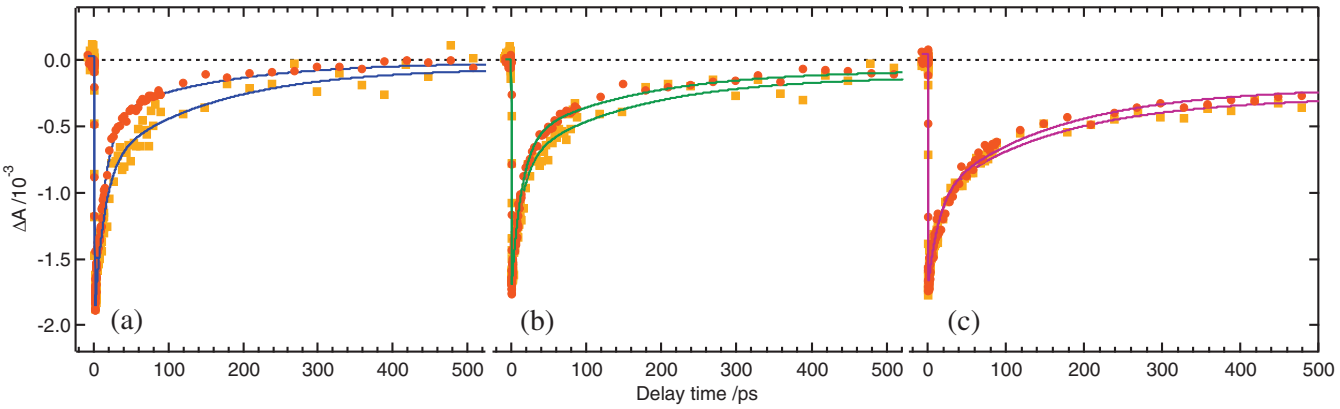

FIGURE 4 Transient decays associated with bands for recombination mediated for direct (a), shallow (b), and deep trap states (c) monitored at 700 (1.77 eV), 850 (1.46 eV), and 1,150 (1.08 eV) nm, respectively, for pristine (■) and photoactivated (●) BiOI nanoplatelet samples. The transient bands were fitted to a double exponential function. The fitted curves for transient decays at 700 (——), 850 (——), and 1,150 (——) nm are shown as solid lines

of the photo-bleach signals of the hot carriers in the NIR region for the photoactivated sample than for the pristine sample. The increased photodoped carrier density of the photoactivated sample is reflected in an increased amplitude of the hot-carrier spectrum shown in Figure S1b. The reason for all spectral bands decaying with the same time coefficients can be understood from the flat structure of the valence bands and a thermal equilibrium between close-lying bands associated with excitons, shallow traps, and deep traps.

A mechanism for carrier relaxation in BiOI samples is shown in Figure 5. BiOI is an indirect band-gap semiconductor in which photoexcitation creates carriers in direct, indirect, shallow, and deep trap states as instantaneous photo-bleach signals are formed at probed regions. Hot carrier cooling occurs for holes and electrons via carrier-carrier annihilation with time coefficient 15 ps. A significant portion of the TA signal recovers through carrier cooling, indicating that both pristine (∼60%) and photo-activated (∼80%) samples have excess background or photodoped carriers due to vacancies. Recombination mediated by a shallow trap state occurs with time coefficient 152 ps; deep trap recombination occurs with time coefficient ∼6 ns. Generally, carriers in

TABLE 1 Curve-fitted results for TA decay bands of pristine and photoactivated BiOI nanoplatelet samples monitored at 1.77, 1.46 and 1.08 eV respectively

	1.77 eV (700 nm)			1.46 eV (850 nm)			1.08 eV (1,150 nm)		
BiOI samples	τ_1/ ps (A_1%)	τ_2/ ps (A_2%)	τ_3/ ps (A_3%)	τ_1/ ps (A_1%)	τ_2/ ps (A_2%)	τ_3/ ps (A_3%)	τ_1/ ps (A_1%)	τ_2/ ps (A_2%)	τ_3/ ps (A_3%)
Pristine	15 (58.6)	152 (37)	6,000 (4.4)	15 (54.9)	152 (36.3)	6,000 (8.8)	15 (36)	152 (46.8)	6,000 (17.2)
Photo activated	15 (78.2)	152 (21.8)	6,000 (0.05)	15 (65.7)	152 (30.6)	6,000 (3.73)	15 (37.7)	152 (47.9)	6,000 (14.4)

Note: The decay bands were fitted to a triple exponential function.

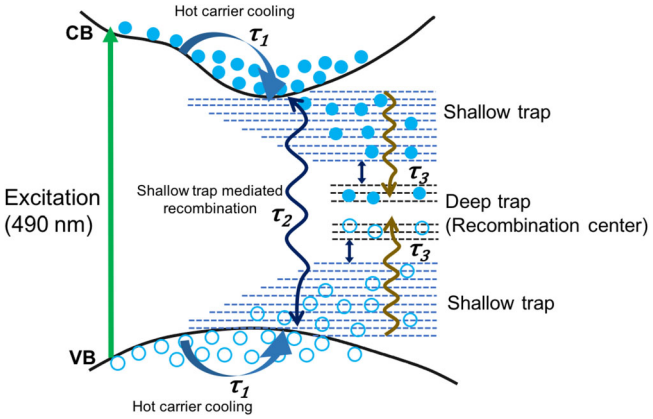

FIGURE 5 Mechanism of carrier relaxation for a BiOI photocatalyst, an indirect bandgap material. Following photoexcitation carriers relax to the indirect band edge with time coefficient τ_1 and further recombine via shallow- and deep trap-mediated recombination paths with time coefficients τ_2 and τ_3, respectively

shallow trap states, which lie in energy near the band edge, decay more slowly than in deep traps, which lie near the Fermi levels as shallow trap recombination involves trapping and detrapping due to thermal equilibrium in the band edge, whereas such processes are inaccessible for deep traps. In the present case, we propose a consecutive relaxation mechanism for a thermal equilibrium established between band edge, shallow trap, and deep trap states; the density of states increases as we move more deeply inside the forbidden region. Such a mechanism of thermal equilibrium should delay the recombination from the deep trap states. Accordingly, we assign τ_1 to hot carrier cooling via carrier-carrier annihilation and τ_2 to shallow (surface)-mediated recombination, which agrees satisfactorily with the assignments and time scales reported for CVD-grown randomly oriented BiOI films. The assignment of τ_3 to deep-trap-mediated recombination associated with oxygen vacancies is also consistent within the ns time scale reported for oxygen-vacancy-mediated recombination for BiOBr nanoplatelets.[19,26] Theoretical calculations indicate that Bi and I vacancies form more easily than O vacancies,[5,26,32] but the pristine sample prepared for this work was an oxygen-rich sample with many adsorbed oxygen atoms, as shown in Figure 2b. It follows that both shallow and deep trap states should be present in both samples because all atoms involved show vacancies in the XPS in Figure 2. The TA spectra and dynamics presented herein hence reveal the role of shallow and deep defects of BiOI in extending the absorption and carrier lifetimes below the bandgap regions, as clearly demonstrated in Figure 5.

3 | CONCLUSIONS

BiOI nanoplatelets with a major occurrence of facet [001] were synthesized with an antisolvent method. The synthesized nanoplatelets showed a tetragonal crystal structure with dimensions length 200–400 nm and thickness less than 50 nm. Photoactivation of nanoplatelets affected neither the crystal structure nor the morphology of the samples. XPS also showed that the synthesized nanoplatelets were robust, as they showed no structural change upon photoactivation of their surfaces except decreased intensities because of the formation of vacancies. Tauc plots obtained after applying a Kubelka-Munk transformation to diffuse reflectance spectra showed that BiOI nanoplatelets belong to indirect-bandgap materials with direct and indirect allowed transitions at 2.19 and 1.83 eV, respectively. Photoactivation of BiOI nanoplatelets shows a slight red shift with direct and indirect allowed transitions at 2.15 and 1.80 eV, respectively. Femtosecond TAS measured in region 2.25–0.9 eV show continuous and indistinguishable broad features associated with band-edge, shallow, and deep trap states due to a close allocation of these states, for both pristine and photoactivated samples. A global fit of the transient spectra shows a consecutive relaxation with three decay coefficients, 15 ps (τ_1), 152 ps (τ_2), and 6 ns (τ_3) for both pristine and photoactivated samples. Photoactivated samples display a greater magnitude of more rapid decay

component (τ_1) than a pristine sample because of photo-doping of bands caused by defects for the former than for the latter. A clear picture is given on hot carrier relaxation proceeding through cooling (τ_1), shallow trap (τ_2), and deep trap (τ_3) energy states.

4 | EXPERIMENTAL SECTION

4.1 | Materials

All materials were used without purification: bismuth iodide (BiI_3, 99%, Sigma Aldrich), *N*,*N*-dimethylformamide (DMF, anhydrous, 99.8%, Sigma Aldrich), 2-propanol (IPA, Sigma Aldrich).

4.2 | Synthesis of BiOI nanoplatelets

BiOI nanoplatelets were synthesized with an antisolvent method. BiI_3 (0.2 mmol) was placed in a glass vial (5 ml) and dissolved in DMF (2 ml) on heating at 70°C until the solution turned orange and transparent. This orange liquid was rapidly injected into IPA (40 ml) maintained under continuous stirring in a spherical flask. After injection, DI water (10 ml) was added to the IPA; the solution was stirred for 10 min. For purification of the solid, the colloidal solution was centrifuged (5,000 rpm, 15 min) to separate BiOI nanoplates. Nanoplatelets were dispersed in IPA and again centrifuged to remove residual DMF. The nanoplatelets were dispersed in IPA for further experiments.

4.3 | Structural and morphological characterizations

X-ray diffraction (XRD) patterns of pristine and photo-irradiated BiOI nanoplatelet powders were obtained with an X-ray diffractometer (Bruker AXS, D8 Advance, Cu Kα irradiation, $\lambda = 154.18$ pm). A field-emission scanning electron microscope (FESEM, Hitachi SU8010) was used to observe the two-dimensional platelet structures of BiOI samples. XPS (Thermo K-α Surface Analysis) provided elemental analysis and surface composition. Drop-cast samples prepared from suspensions of BiOI particles dispersed in IPA on an indium-titanium-oxide (ITO) substrate were used for XPS experiments.

4.4 | Optical methods

Diffuse reflectance spectra of pristine and photo-irradiated BiOI samples were recorded in the visible and NIR regions (JASCO spectrophotometer V-780, equipped with an integration sphere, ISN-9011, JASCO). Data analysis was performed on recorded reflectance spectra with Kubelka-Munk transformations and Tauc plots to estimate the absorption spectra and band gaps of these samples. Femtosecond transient absorption (TAS) was measured in the visible and NIR regions with a pump-probe spectrometer (ExciPro, CDP) in combination with a femtosecond Ti-sapphire-amplified laser system (Coherent, Legend USP, 1 kHz, 795 nm, 3 mJ, 45 fs). Excitation wavelengths for pump and probe were generated using optical parametric amplifiers (TOPAS). BiOI nanoplatelet powder samples cast on a circular glass (25 mm, BK7) substrate of thickness 1 mm were excited with light at 490 nm and pulse energy 0.2 mJ/cm^2. The samples were probed in the visible and NIR regions using a white-light supercontinuum generated from a sapphire crystal of thickness 5 mm. The pump wavelengths were set to 1,300 and 800 nm to generate a white-light continuum in the visible and NIR regions. The pump light and second-order light were blocked with appropriate bandpass filters. Pump-probe experiments in the visible region were performed using a Si array detector, whereas an InGaAs array detector was used for NIR experiments (1,000–1,300 nm). The polarization between pump and probe was set to a magic angle.

ACKNOWLEDGMENTS

EWGD thanks Professor Y.-P. Lee, who celebrates his 70th birthday on this occasion, for his strong support in research of fundamental science developed in NYCU. Taiwan Ministry of Science and Technology (MOST 109-2123-M-009-001 and MOST 110-2634-F-009-026) and Center for Emergent Functional Matter Science of National Yang Ming Chiao Tung University (NYCU) from The Featured Areas Research Center Program within the framework of the Higher Education Sprout Project by Taiwan Ministry of Education (MOE) supported this research.

REFERENCES

[1] M. D. Prasad, G. V. Ramesh, S. K. Batabyal, *ACS Sym. Ser.* **2020**, *1353*, 295.
[2] J. Di, J. Xia, H. Li, S. Guo, S. Dai, *Nano Energy* **2017**, *41*, 172.
[3] B. Liu, Y. Wang, P. Chen, X. Zhang, H. Sun, Y. Tang, Q. Liao, J. Huang, H. Wang, H. Meng, X. Guo, *ACS Appl. Mater. Inter.* **2019**, *11*, 33505.
[4] A. Crovetto, A. Hajijafarassar, O. Hansen, B. Seger, I. Chorkendorff, P. C. K. Vesborg, *Chem. Mater.* **2020**, *32*, 3385.
[5] R. L. Z. Hoye, P. Schulz, L. T. Schelhas, A. M. Holder, K. H. Stone, J. D. Perkins, D. Vigil-Fowler, S. Siol, D. O. Scanlon, A. Zakutayev, A. Walsh, I. C. Smith, B. C. Melot, R. C. Kurchin, Y. Wang, J. Shi, F. C. Marques, J. J. Berry, W. Tumas, S. Lany, V. Stevanović, M. F. Toney, T. Buonassisi, *Chem. Mater.* **2017**, *29*, 1964.

[6] X. Sun, H. Huang, Q. Zhao, T. Ma, L. Wang, *Adv. Funct. Mater.* **2020**, *30*, 1910005.
[7] L. Wang, L. Wang, Y. Du, X. Xu, S. X. Dou, *Mater. Today Phys.* **2021**, *16*, 100294.
[8] B. Long, Y. Huang, H. Li, F. Zhao, Z. Rui, Z. Liu, Y. Tong, H. Ji, *Ind. Eng. Chem. Res.* **2015**, *54*, 12788.
[9] J. Di, J. Xia, M. Ji, B. Wang, S. Yin, H. Xu, Z. Chen, H. Li, *Langmuir* **2016**, *32*, 2075.
[10] R. A. Jagt, T. N. Huq, K. M. Börsig, D. Sauven, L. C. Lee, J. L. MacManus-Driscoll, R. L. Z. Hoye, *J. Mater. Chem. C* **2020**, *8*, 10791.
[11] M. D. Prasad, M. G. Krishna, S. K. Batabyal, *ACS Appl. Nano Mater.* **2019**, *2*, 3906.
[12] X. Zhang, Z. Ai, F. Jia, L. Zhang, *J. Phys. Chem. C* **2008**, *112*, 747.
[13] J. Hou, K. Jiang, M. Shen, R. Wei, X. Wu, F. Idrees, C. Cao, *Sci. Rep.* **2017**, *7*, 11665.
[14] M. A. M. Yusoff, S. S. Imam, I. Shah, R. Adnan, *Mater. Res. Express* **2019**, *6*, 0850g5.
[15] L. Ye, X. Jin, X. Ji, C. Liu, Y. Su, H. Xie, C. Liu, *Chem. Eng. J.* **2016**, *291*, 39.
[16] L. Ye, L. Zan, L. Tian, T. Peng, J. Zhang, *Chem. Commun.* **2011**, *47*, 6951.
[17] Z. Wang, Z. Chu, C. Dong, Z. Wang, S. Yao, H. Gao, Z. Liu, Y. Liu, B. Yang, H. Zhang, *ACS Appl. Nano Mater.* **2020**, *3*, 1981.
[18] Y. Huang, Y. Yu, Y. Yu, B. Zhang, *Sol. RRL* **2020**, *4*, 2000037.
[19] H. Wang, D. Yong, S. Chen, S. Jiang, X. Zhang, W. Shao, Q. Zhang, W. Yan, B. Pan, Y. Xie, *J. Am. Chem. Soc.* **2018**, *140*, 1760.
[20] M. Ai, J. Zhang, Y. Wu, L. Pan, C. Shi, J. Zou, *Chem. Asian J.* **2020**, *15*, 3599.
[21] J. Xiong, J. Di, J. Xia, W. Zhu, H. Li, *Adv. Funct. Mater.* **2018**, *28*, 1801983.
[22] M. Shen, T. Ding, J. Luo, C. Tan, K. Mahmood, Z. Wang, D. Zhang, R. Mishra, M. D. Lew, B. Sadtler, *J. Phys. Chem. Lett.* **2020**, *11*, 5219.
[23] X. Tao, W. Shi, B. Zeng, Y. Zhao, N. Ta, S. Wang, A. A. Adenle, R. Li, C. Li, *ACS Catal.* **2020**, *10*, 5941.
[24] A. Yamakata, J. J. M. Vequizo, H. Matsunaga, *J. Phys. Chem. C* **2015**, *119*, 24538.
[25] R. Katoh, M. Murai, A. Furube, *Chem. Phys. Lett.* **2008**, *461*, 461.
[26] T. N. Huq, L. C. Lee, L. Eyre, W. Li, R. A. Jagt, C. Kim, S. Fearn, V. Pecunia, F. Deschler, J. L. MacManus-Driscoll, R. L. Z. Hoye, *Adv. Funct. Mater.* **2020**, *30*, 1909983.
[27] X. Zhang, X.-B. Wang, L.-W. Wang, W.-K. Wang, L. Long, W.-W. Li, H.-Q. Yu, *ACS Appl. Mater. Inter.* **2014**, *6*, 7766.
[28] D. Zhang, L. Chen, T. Wei, C. J. Xiao, Z. Q. Wang, *Adv. Mat. Res.* **2015**, *1095*, 72.
[29] A. Escobedo-Morales, I. I. Ruiz-López, M. D. L. Ruiz-Peralta, L. Tepech-Carrillo, M. Sánchez-Cantú, J. E. Moreno-Orea, *Heliyon* **2019**, *5*, e01505.
[30] P. Makuła, M. Pacia, W. Macyk, *J. Phys. Chem. Lett.* **2018**, *9*, 6814.
[31] J. F. Florez-Rios, M. A. Santana-Aranda, J. G. Quiones-Galvn, A. Escobedo-Morales, A. Chvez-Chvez, A. Prez-Centeno, *Mater. Res. Express* **2020**, *7*, 015912.
[32] R. L. Z. Hoye, L. C. Lee, R. C. Kurchin, T. N. Huq, K. H. L. Zhang, M. Sponseller, L. Nienhaus, R. E. Brandt, J. Jean, J. A. Polizzotti, A. Kursumović, M. G. Bawendi, V. Bulović, V. Stevanović, T. Buonassisi, J. L. MacManus-Driscoll, *Adv. Mater.* **2017**, *29*, 1702176.
[33] V. Pecunia, J. Zhao, C. Kim, B. R. Tuttle, J. Mei, F. Li, Y. Peng, T. N. Huq, R. L. Z. Hoye, N. D. Kelly, S. E. Dutton, K. Xia, J. L. MacManus-Driscoll, H. Sirringhaus, *Adv. Energy. Mater.* **2021**, *11*, 2003968.

AUTHOR BIOGRAPHIES

Atul H. Bhosale received his MS degree in physics from Savitribai Phule Pune University in 2018. Currently, he is a PhD student under the supervision of Prof. Eric Wei-Guang Diau in National Yang Ming Chiao Tung University. His research interests are investigations of carrier relaxation dynamics of photocatalysts and halide perovskite semiconductor materials applied in photocatalytic, photovoltaic and optoelectronic applications using ultrafast transient absorption spectroscopy.

Sudhakar Narra received his doctoral degree in Physical Chemistry from the Department of Applied Chemistry, National Chiao Tung University in the year 2014 under the supervision of Prof. Shinsuke Shigeto. Currently, he is working as a postdoctoral researcher at the same university. His research interests are structural studies, dynamics and electric field effects on functional materials using ultrafast optical spectroscopy.

Sumit S. Bhosale received his PhD in Applied Chemistry from National Chiao Tung University in 2020, under the supervision of Prof. Eric Wei-Guang Diau. Currently he is a postdoctoral fellow at National Yang Ming Chiao Tung University. His research interests focus on application of semiconductor quantum dots for photovoltaic, photocatalytic and optoelectronic applications.

Po-Sen Liao completed his undergraduate studies from the Department of Chemistry, National Central University in 2019. Currently he is pursuing his master degree from Graduate Program of Molecular Science, Department of Applied Chemistry in National Yang Ming Chiao Tung University

under the supervision of professor Eric Wei-Guang Diau. His research interests are to understand photochemistry and photophysics of perovskite nanocrystals and other optoelectronic materials using ultrafast optical spectroscopy.

Nobuhiro Ohta is currently a Chair Professor at Department of Applied Chemistry/Institute of Molecular Science and Center for Emergent Functional Matter Science, National Yang Ming Chiao Tung University (NYCU), Taiwan, and Professor Emeritus at Hokkaido University, Japan. Before joining NYCU, he was a Professor at Research Institute for Electronic Science, Hokkaido University, Japan. His research interests are electric field effects on structure, dynamics and function of molecules, optoelectronic materials and live cells.

Eric Wei-Guang Diau started his research in 2001 in Department of Applied Chemistry and Science of Molecular Science, National Chiao Tung University (NCTU), Taiwan. His current research is focusing on the developments of novel perovskites and functional materials for applications in photovoltaics, photocatalysis, light emitting diode, display, and so on. He received "Sun Yat Sen Academic Award" in 2014, "MOST Outstanding Research Award" in 2018 and "17th Hsu Yu-Ziang Science Paper Award" in 2019. He has published over 210 peer-reviewed papers with H-index 65. He is currently Distinguished Professor at Department of Applied Chemistry of National Yang Ming Chiao Tung University (NYCU), Taiwan.

SUPPORTING INFORMATION

Additional supporting information may be found online in the Supporting Information section at the end of this article.

How to cite this article: A. H. Bhosale, S. Narra, S. S. Bhosale, P.-S. Liao, N. Ohta, E. W.-G. Diau, *J. Chin. Chem. Soc.* **2022**, *69*(1), 51. https://doi.org/10.1002/jccs.202100279